# NUMERICAL AND EXPERIMENTAL BENCHMARKING OF MICROBUNCHING INSTABILITY WITH INTRABEAM SCATTERING IN LINAC-FELS

S. Di Mitri[1,2,*], G. Campri[1], F. Elisii[2], G. Perosa[3], S. Spampinati[1]
[1] Elettra Sincrotrone Trieste, I-34149 Basovizza, Trieste
[2] University of Trieste, Dept. Physics, V. A. Valerio I-34100 Trieste
[3] European XFEL GmbH, Holzkoppel 4, G-22869, Schenefeld

*Abstract*

The benchmark of a semi-analytical model of microbunching instability affecting electron beams in single pass or recirculating linear accelerators with experimental data published in the literature is reported. The model is comprehensive of numerous features of the instability, such as low and high gain contributions, either linearized or at second order, coherent synchrotron and edge radiation, Landau damping by transverse emittance and laser heater, for single and double magnetic bunch length compression. The model is enriched by three different expressions to calculate intrabeam scattering. The inclusion of this effect allows the recovery of agreement with published experimental observations, to date either in disagreement with theory, or in partial agreement by virtue of blind fitting of parameters.

## INTRODUCTION

In single pass or recirculating electron linear accelerators (linacs), microbunching instability (MBI) is the beam collective effect causing dilution of the longitudinal phase space by the amplification of energy and density modulations in succession [1]. The instability is one of the potential show-stoppers to longitudinal coherence at the Fourier limit level of linac-driven XUV free-electron lasers (FELs). In particular, it has been recognized at the origin of radiation pedestal and power reduction in X-ray self-seeded FELs [2], and of sidebands in externally-seeded EUV FELs [3,4]. In general, the instability determines FEL bandwidth enlargement and reduction of the spectral flux, in proportion to the harmonic jump of lasing.

The instability is seeded by the granularity of the electron distribution, possibly in combination with narrowband phase space structures originated in radiofrequency (RF) photo-injectors [5,6]. The nature of the initial modulations, in combination with some damping mechanisms, commonly bounds the instability to final wavelengths in the range ~0.1–10's μm, hence the naming.

The spread of particles' path length in dispersive regions, due to either chromatic or betatron motion, washes out modulations at the shortest wavelengths of the broadband instability spectrum, in fact putting in place longitudinal and transverse Landau damping [7]. Transverse damping can be enhanced by optics tuning for an enlarged curl-$H_x$ function [8], while the betatron emittance is preserved. Longitudinal damping is usually more effective than the transverse. It is more effective for larger beam uncorrelated energy spread, and this is in most cases increased by a laser heater system [9] in the low energy region of the linac, well before the instability builds up. In this case, however, the enlargement of the beam longitudinal emittance imposes a tradeoff between FEL spectral purity and intensity [10,11]. Additional damping mechanisms have been identified in the folding of phase space at high energy (phase mixing) [12] and, recently first observed in an electron linac, intrabeam scattering (Landau damping) [13].

At least three semi-analytical approaches to model MBI have been developed in the last two decades, which can be shortly referred to as, respectively, integral linearized Vlasov-Maxwell equation [14], matrix multiplication [15], and linearized Vlasov-Poisson equation in a plasma [16,17]. In the following, we will adopt the first one; for the sake of brevity, we will name it Huang-Kim (HK), with reference to the authors who, after the conceptualization by Saldin *et al.* in [9], first introduced the formalisms with prescriptions for a numerical implementation. The model is basically time-independent (it describes the bunch core slice dynamics), valid in ultra-relativistic regime. The use of effective transverse beam sizes in the calculation of Coulomb interactions justifies 1.5-D approximations to some extent [18].

The Reader is kindly sent to [19] for a systematic report on the numerical benchmark of the Huang-Kim and the Bosch-Kleman-Wu (BKW) semi-analytical models of MBI. Here, we show that the inclusion of intrabeam scattering (IBS) is essential to the recovery of agreement with published experimental observations, to date either in disagreement with theory, or in partial agreement by virtue of blind fitting of parameters.

## BENCHMARK OF MEASUREMENTS

### *FERMI High Charge*

The HK formalism was successfully applied in [13] to explain the observed ~100 keV slice energy spread at the end of the FERMI linac in a low charge regime (100 pC), for which IBS was shown to play a critical role in limiting the MBI gain. The exercise is repeated here for the slice energy spread measured at the same facility in high charge regime (600 pC), and reported in Fig.2 of [20].

†simone.dimitri@eletra.eu

Figure 1 compares $\sigma_{E,tot}$ predicted by HK and BKW to the slice energy spread $\sigma_{E,m}$ measured at the entrance of the FERMI FEL undulator line, at the energy of 1.32 GeV, for the three peak currents of 0.8, 1.1 and 1.3 kA. The comparison is carried out for no heating and for heating inducing 5 keV RMS energy spread (approximately 1 μJ pulse energy). The modelling includes the 25 m-long FERMI high energy transfer line connecting the linac to the undulator: it is treated as a straight section, neglecting its small $|R_{56}| < 1$ mm and hence CSR in the four dipoles, while LSC and IBS are included. Doing so, the present modelling is missing the potential impact of phase mixing, energy or emittance damping developing through the transfer line.

The initial peak current is estimated $\sim 600pC/8ps = 75\,A$, and thereby the compression factor in BC1 results $C \cong 11$ (0.8 kA), 15 (1.1 kA) and 17 (1.3 kA). By assuming that $\sigma_{E,m}$ with no heating is weakly affected by the instability, the uncorrelated energy spread at the entrance of BC1, at the beam energy of 300 MeV, is estimated as the minimum among the values $\sigma_{E,BC1} = \min(\sigma_{E,m}/C) = min(3.0, 3.3, 3.7) = 3.0$ keV, where $\sigma_{E,m}$= 41, 50, 53 keV respectively. To retrieve the uncorrelated energy spread at the exit of the photo-injector, ~20 m upstream BC1 and at the beam energy of 100 MeV, we subtract in quadrature from $\sigma_{E,BC1}$ the minimum energy spread induced by IBS along that region, *i.e.* 1.8 keV, and eventually fix the initial energy spread to $\sigma_{E,0} = 2.4$ keV.

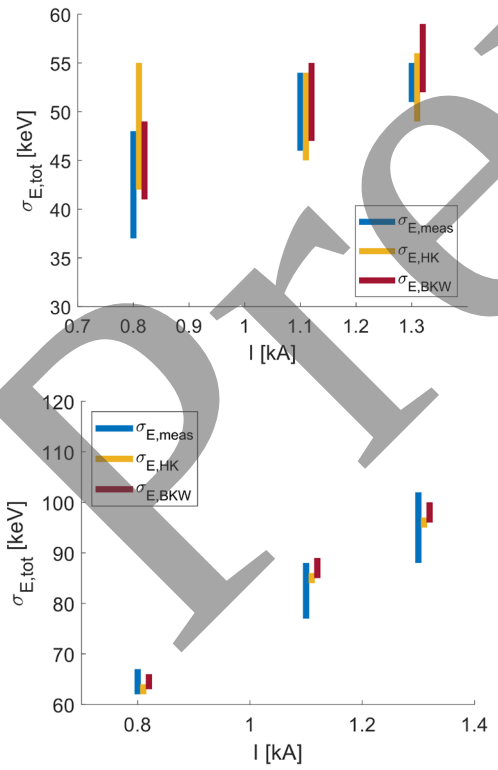


Figure 1: Slice energy spread at the entrance of the FERMI undulator line predicted by HK (orange), BKW (red), and measured [20] (blue), for laser heater off (top) and inducing 5 keV RMS energy spread (bottom).

Figure 1 confirms the mutual agreement of HK and BKW, and of their prediction with measurements [20], with and without beam heating. The height of the vertical blue bars corresponds to the experimental uncertainty reported in [20]. The height of the orange and red bars corresponds to the peak-to-peak variation of the prediction over all three IBS models introduced in [19], and for average betatron functions along the FERMI beam line scanned in the range 10–20 m. It is worth stressing that the models do not imply any fitting procedure.

We observe that the prediction becomes more and more insensitive to IBS and beam optics when the instability is largely damped by the laser heater (shorter orange and red bars in the bottom plot). Unlike for the low charge regime reported in [13], the final energy spread is here basically the same with and without IBS, apart for a redistribution of the intrinsic and MBI-induced energy spread along the line. This is confirmed independently from the IBS model adopted. The maximum deviation in the final energy spread, for any given linac configuration, is less than 2 keV. CSR, low gain terms and nonlinear gain all contribute to the increase of the final energy spread by less than 3% (not shown).

*LCLS Low Charge*

In some cases, the inclusion of IBS is crucial to a reliable prediction of the MBI gain and thereby of the final slice energy spread. This is also shown to be the case in Fig.2, where the prediction from HK theory, with IBS and without it (dashed line, orange circle), is compared to LCLS experimental data reported in [21]. A 180-pC bunch charge is compressed in two-stage to 1 kA ($C \cong 35$). The final energy is 4.3 GeV, the initial uncorrelated energy spread is $\sigma_{E,0} = 1$ keV.

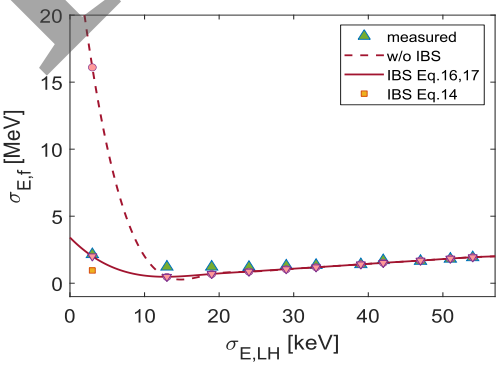


Figure 2: Final slice energy spread as function of laser-induced energy spread at the LCLS. Experimental data (upper green triangles) are from [21]. Orange symbols are from HK, in correspondence of the experimental data, and they superimpose for $\sigma_{E,LH} > 10$ keV (only lower triangles shown for illustration). In particular, solid line and lower triangles are for IBS as in Eq.16 and 17 in [19] (the two IBS models provide the same final energy spread to any meaningful numerical accuracy). Dashed line and circles are from HK without IBS. Squares are from HK with IBS as in Eq.14 in [19].

For $\sigma_{E,LH} > 10$ keV, the instability is largely damped, $\sigma_{E,IBS}, \sigma_{E,MBI} \ll C\sigma_{E,LH}$, and therefore one finds $\sigma_{E,f} \cong C\sigma_{E,LH}$. At low beam heating, instead, the measured data can only be recovered by including Landau damping from IBS (compare dashed and solid line; the deviation in the absence of IBS is not due to the approximation of linear gain, as initially supposed in [21]).

*SwissFEL Low Charge*

The proposed modelling of MBI is further tested against experimental data of slice energy spread collected at the SwissFEL for an uncompressed 200 pC charge bunch, see Fig.3. The experiment is reported in [22], as function of the laser heater chicane $R_{56}$, for the downstream BC1 chicane turned off and on, but still $C = 1$. The theoretical benchmark of measurements proposed in [22] adopts the IBS model in Eq.14 in [19], but with the Coulomb logarithm scaled by a fitting coefficient $\alpha = 2.4$. It is shown below that the models proposed in Eqs.14,16,17 in [19] provide a similarly good agreement with the observations, without the need of any fitting.

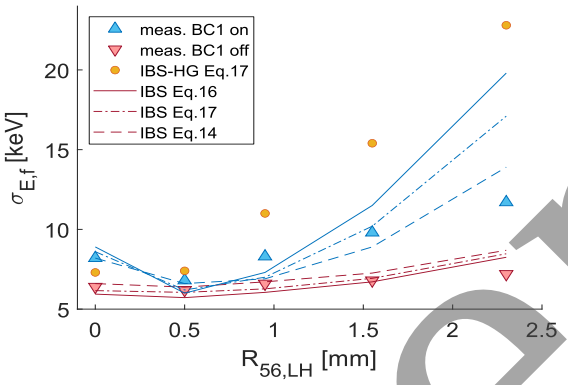


Figure 3: Final slice energy spread as function of $R_{56,LH}$ at the SwissFEL. Experimental data with BC1 chicane turned on (upper blue triangles) and off (lower red triangles) are taken from Fig.6 in [22]. Theoretical data including IBS are from HK with (blue lines for BC1 turned on, red lines for BC1 turned off) and without low gain terms (orange circles, BC1 turned on).

Since the proposed IBS theory is derived for ultra-relativistic beams, the SwissFEL beam line is modelled here as an initial short drift section at 150 MeV, followed by the laser heater chicane, then a linac accelerating to 300 MeV up to BC1, and eventually the diagnostic line. To take into account the possible impact of IBS from the Gun to the laser heater area, and following [22], an initial energy spread of 4 keV at 150 MeV is assumed. The change in beam optics downstream BC1 when the chicane is turned off is implemented as an effective 30% average larger beam size.

The predictions in Fig.3 (lines) well reflect the observed minimum of slice energy spread for $R_{56,LH} = 0.5$ mm (upper triangles). The analysis reveals that the minimum (also barely noticeable for BC1 tuned off, lower triangles) shows up by virtue of the cancellation of low and high gain terms [19], in correspondence of which the peak gain lowers to 60 at the wavelength of 8 μm (not shown). To demonstrate this, the energy spread predicted by using Eq.17 in [19] without low gain terms and BC1 turned on is also shown with orange circles (to be compared with upper triangles and dash-dotted blue line).

## CONCLUSION

The proposed implementations of HK and BKW both allow, within the aforementioned numerical uncertainties and well within the experimental ones, the recovery of agreement of predicted and measured slice energy spread in cases so far never benchmarked with theory [20], in disagreement with theory lacking IBS [21], or in partial agreement by virtue of blind fitting of IBS parameters [2]. In the latter case, the analysis reveals the fundamental contribution of low gain terms to the minimization of the energy spread as function of the laser heater chicane's $R_{56}$.

We conclude that, in spite of several approximations and effective beam models, the presented implementations of HK and BKW formalism are equivalently capable of capturing the salient MBI physics in a wide range of operational parameters of XUV FELs. While the absolute numerical accuracy of the predicted gain and energy spread certainly depends, for example, from the accuracy of the experimental data for the beam parameters at the injector exit and for the beam optics along the line, the models result well suited for a global optimization of the linac setting in the presence of MBI. In general, the inclusion of low gain terms and of IBS according to Eq.16 or 17 in [19] is recommended.

## REFERENCES


[1] Z. Huang and G. Stupakov, "Control and application of beam microbunching in high brightness linac-driven free electron lasers," *Nucl. Instrum. Methods Phys. Res., Sect. A*, vol. 907, pp. 182–187, Nov. 2018. doi:10.1016/j.nima.2018.02.030

[2] G. Marcus *et al.*, "Experimental observations of seed growth and accompanying pedestal contamination in a self-seeded, soft x-ray free-electron laser," *Phys. Rev. Accel. Beams*, vol. 22, no. 8, Aug. 2019. doi:10.1103/physrevaccelbeams.22.080702

[3] P. Rebernik Ribič *et al.*, "Coherent soft X-ray pulses from an echo-enabled harmonic generation free-electron laser," *Nat. Photonics*, vol. 13, no. 8, pp. 555–561, May 2019. doi:10.1038/s41566-019-0427-1

[4] N. S. Mirian *et al.*, "Characterization of soft x-ray echo-enabled harmonic generation free-electron laser pulses in the presence of incoherent electron beam energy modulations," *Phys. Rev. Accel. Beams*, vol. 24, no. 8, Aug. 2021. doi:10.1103/physrevaccelbeams.24.080702

[5] P. Emma, Z. Huang, J. Wu, M. Borland, and C. Limborg, "Temporal Profile of the LCLS Photocathode Ultraviolet Drive Laser Tolerated by the Microbunching Instability", in *Proc. LINAC'04*, Lübeck, Germany, Aug. 2004, paper TUP53, pp. 390-392.

[6] S. Bettoni *et al.*, "Impact of laser stacking and photocathode materials on microbunching stability in photoinjectors," *Phys. Rev. Accel. Beams*, vol. 23, no. 2, Feb. 2020. doi:10.1103/physrevaccelbeams.23.024401

[7] J. Qiang, C. E. Mitchell, and M. Venturini, "Suppression of Microbunching Instability Using Bending Magnets in Free-Electron-Laser Linacs," *Phys. Rev. Lett.*, vol. 111, no. 5, Jul. 2013. doi:10.1103/physrevlett.111.054801

[8] A. D. Brynes *et al.*, "Mitigation of the microbunching instability through transverse Landau damping," *Phys. Rev. Accel. Beams*, vol. 27, no. 7, Jul. 2024. doi:10.1103/physrevaccelbeams.27.074402

[9] E. L. Saldin, E. A. Schneidmiller, and M. V. Yurkov, "Longitudinal space charge-driven microbunching instability in the TESLA Test Facility linac," in Free Electron Lasers 2003, Ed., 2004, pp. 355–359. doi:10.1016/b978-0-444-51727-2.50081-x

[10] Z. Huang *et al.*, "Measurements of the linac coherent light source laser heater and its impact on the x-ray free-electron laser performance," Physical Review Special Topics - Accelerators and Beams, vol. 13, no. 2, Feb. 2010. doi:10.1103/physrevstab.13.020703

[11] S. Spampinati *et al.*, "Laser heater commissioning at an externally seeded free-electron laser," *Phys. Rev. Spec. Top. Accel Beams*, vol. 17, no. 12, Dec. 2014. doi:10.1103/physrevstab.17.120705

[12] S. Di Mitri and S. Spampinati, "Microbunching Instability Suppression via Electron-Magnetic-Phase Mixing," *Phys. Rev. Lett.*, vol. 112, no. 13, Apr. 2014. doi:10.1103/physrevlett.112.134802

[13] S. Di Mitri *et al.*, "Experimental evidence of intrabeam scattering in a free-electron laser driver," *New J. Phys.*, vol. 22, no. 8, p. 083053, Aug. 2020. doi:10.1088/1367-2630/aba572

[14] Z. Huang and K.-J. Kim, "Erratum: Formulas for coherent synchrotron radiation microbunching in a bunch compressor chicane [Phys. Rev. ST Accel. Beams5, 074401 (2002)]," Physical Review Special Topics - Accelerators and Beams, vol. 5, no. 12, Dec. 2002. doi:10.1103/physrevstab.5.129903

[15] R. A. Bosch, K. J. Kleman, and J. Wu, "Modeling two-stage bunch compression with wakefields: Macroscopic properties and microbunching instability," Physical Review Special Topics - Accelerators and Beams, vol. 11, no. 9, Sep. 2008. doi:10.1103/physrevstab.11.090702

[16] A. Marinelli, E. Hemsing, and J. B. Rosenzweig, "Three dimensional analysis of longitudinal plasma oscillations in a thermal relativistic electron beam," *Phys. Plasma*, vol. 18, no. 10, Oct. 2011. doi:10.1063/1.3638139

[17] V. N. Litvinenko *et al.*, "Plasma-cascade instability," *Phys. Rev. Accel. Beams*, vol. 24, no. 1, Jan. 2021. doi:10.1103/physrevaccelbeams.24.014402

[18] M. Venturini, "Models of longitudinal space-charge impedance for microbunching instability," Physical Review Special Topics - Accelerators and Beams, vol. 11, no. 3, Mar. 2008. doi:10.1103/physrevstab.11.034401

[19] S. Di Mitri, G. Campri, F. Elisii, G. Perosa, and S. Spampinati, "Systematic and comprehensive comparison of two semianalytical models of microbunching instability," *Phys. Rev. Accel. Beams*, vol. 28, no. 4, Apr. 2025. doi:10.1103/physrevaccelbeams.28.044401

[20] G. Penco *et al.*, "Enhanced seeded free electron laser performance with a "cold" electron beam," *Phys. Rev. Accel. Beams*, vol. 23, no. 12, Dec. 2020. doi:10.1103/physrevaccelbeams.23.120704

[21] D. Ratner *et al.*, "Time-resolved imaging of the microbunching instability and energy spread at the Linac Coherent Light Source," Physical Review Special Topics - Accelerators and Beams, vol. 18, no. 3, Mar. 2015. doi:10.1103/physrevstab.18.030704

[22] E. Prat *et al.*, "Energy spread blowup by intrabeam scattering and microbunching at the SwissFEL injector," *Phys. Rev. Accel. Beams*, vol. 25, no. 10, Oct. 2022. doi:10.1103/physrevaccelbeams.25.104401